Self-Diffusion of Acetonitrile in a Covalent Organic Framework: Simulation and Experiment

Lars Grunenberg, [†,a,b] Christopher Keßler, [†,c] Tiong Wei Teh,[c] Robin Schuldt,[d] Fabian Heck,[a,b] Johannes Kästner,[d] Joachim Groß,[c] Niels Hansen[c,*] and Bettina V. Lotsch.[a,b,e,*]

---

[a] Max Planck Institute for Solid State Research, Heisenbergstr. 1, 70569 Stuttgart, Germany

[b] Department of Chemistry, Ludwig-Maximilians-Universität (LMU), Butenandtstr. 5-13, 81377 Munich, Germany

[c] Institute of Thermodynamics and Thermal Process Engineering, University of Stuttgart, Pfaffenwaldring 9, 70569 Stuttgart, Germany

[d] Institute for Theoretical Chemistry, University of Stuttgart, Pfaffenwaldring 55, 70569 Stuttgart, Germany

[e] E-conversion, Lichtenbergstrasse 4a, 85748 Garching, Germany

[†] Authors contributed equally.

[*] Email: hansen@itt.uni-stuttgart.de and b.lotsch@fkf.mpg.de
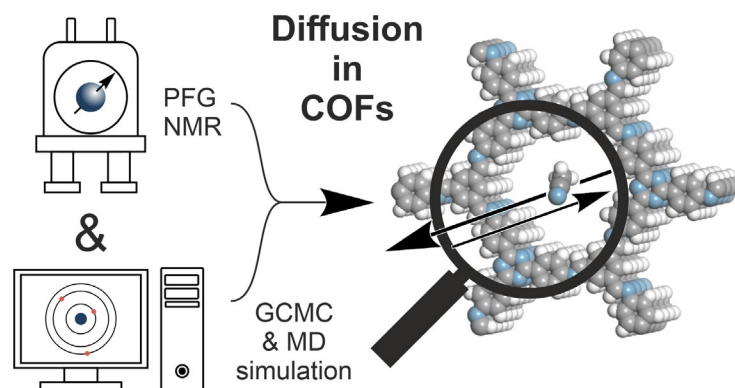
Keywords: Pulsed field gradient NMR, Diffusion, Covalent Organic Framework, Molecular Dynamics, Grand Canonical Monte Carlo

Abstract

Covalent Organic Frameworks have emerged as a new class of porous materials whose sorption properties have so far been studied primarily with physisorption techniques. Quantifying the self-diffusion of guest molecules in the interior of their nanometer-sized pores allows for a better understanding of confinement effects or transport limitations and is thus vital for various applications ranging from molecular separation to catalysis. Using a combination of pulsed field gradient nuclear magnetic resonance (PFG NMR) measurements and molecular dynamics (MD) simulations we have probed the self-diffusion of acetonitrile in the 1.7 nm diameter pore channels of two imine-linked COFs (PI-3-COF) featuring different levels of crystallinity and porosity, between 270 K and 300 K. In the sample showing higher crystallinity and porosity, we observe clear evidence for anisotropic diffusion parallel to the pore channel direction as characterized by a diffusion coefficient of D_{par} = 6.1 × 10^{-10} m^{2}s^{-1} at T = 300 K, consistent with 1D transport. Self-diffusion in the pores vs. bulk liquid is thus reduced by a factor of 7.4, in good agreement with MD simulations which predict a reduction of the self-diffusion coefficient by a factor of 5.4 compared to the bulk liquid value, assuming an offset-stacked COF layer arrangement. In contrast, more frequent diffusion barriers give rise to isotropic, yet significantly reduced diffusivities in the low-porosity sample (D_B = 1.4 × 10^{-11} m^{2}s^{-1} at T = 300 K). Our multimodal study thus highlights the significant influence of real structure effects such as stacking faults and grain boundaries on the long-range diffusivity of molecular guest species, while suggesting efficient intracrystalline transport at short diffusion times.

Introduction

2D covalent organic frameworks (COFs) are a unique class of materials which combine a high level of tunability with intrinsic structural porosity on a crystalline, covalently linked polymeric backbone. Their chemical structure can be tuned with atomic precision, rendering these materials an attractive scaffold for diverse applications, including gas storage and separation, sensing, electrochemical energy storage, and heterogeneous (photo)catalysis.[1-9]

The typically large specific surface areas of these materials, and in particular the spatial arrangement of building blocks as encoded in the shape of the pore channels featuring adjustable diameters in the nanometer range, enables the utilization of confinement effects in heterogeneous catalysis, similar to those well-known from enzymes as biological catalysts.[10] Spatial confinement in these pores allows a precise arrangement and relative orientation of catalytic centers and substrates in the pore channels and modulates the local concentration of reactants in the cavities.[11, 12] These effects can be used as a handle to tailor product selectivity in catalytic reactions, e.g. by suppressing oligomerization in L-lactide synthesis from lactic acid.[13] Recently, Emmerling *et al*. demonstrated that the ordered structural porosity of COFs enhances selectivity for (mono)macrocyclization during a ruthenium catalyzed olefin metathesis reaction, favoring ring closing over oligomerization.[14] While the variation of pore size forms the basis for these effects, interactions between the reactants as well as other molecules in the reaction mixture with the pore wall, become more dominant with a reduction in pore size.[15] Acid/base interactions between catalytic substrates and reaction intermediates can affect the reaction rate, while collision events with the pore walls alter the in- and

3

outflow of reactants.[16, 17] This can lead either to localized concentration gradients affecting selectivity or, in the limiting case for very small pore diameters that exclude (competing) molecules entirely, open up further areas of application, such as molecular sieving or nanofiltration.[18-22]

Computer simulations are well established in the field of porous media. Molecular dynamics (MD) simulations are a versatile tool to study self- and collective diffusion in crystalline porous media such as zeolites, MOFs and COFs[23] or carbon nanotubes,[24] but also in complex amorphous materials if a reasonable structural model is available.[25] In contrast to zeolites[26-30] and MOFs,[31-34] the investigation of self-diffusion in COFs so far focused on light gases such as hydrogen, nitrogen, carbon dioxide, methane and ethane.[35-39] Molecular simulations in conjunction with experimental investigations has led to a fundamental understanding of nano-confinement effects,[40] but such combined studies so far exclusively focused on MOFs[41] and zeolites[42]. Therefore, we herein present a combined experimental and computational study of the self-diffusion of acetonitrile in the two-dimensional covalent organic network PI-3-COF using Pulsed Field Gradient Nuclear Magnetic Resonance (PFG-NMR) spectroscopy and Grand Canonical Monte Carlo (GCMC) and MD simulations. Using two samples with identical composition but differences in their real structure effects (i.e. crystallinity and porosity), we demonstrate the influence of pore confinement on the diffusivities of molecular probes.

4

Results

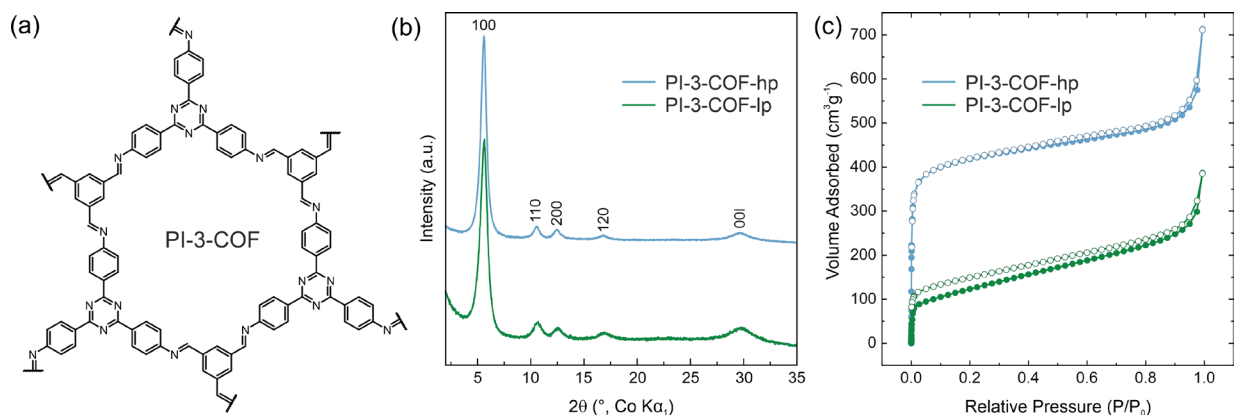## Synthesis and Characterization of COFs

Figure 1: (a) Chemical structure of a single pore of PI-3-COF. (b) XRPD pattern and (c) N$_2$ adsorption isotherm comparison of PI-3-COF-lp (green) and PI-3-COF-hp (blue).

Imine-linked PI-3-COF has been synthesized from 1,3,5-triformyl benzene and 4,4′,4″-(1,3,5-triazine-2,4,6-triyl)trianiline under solvothermal conditions, according to a previously reported procedure.[43] We synthesized two samples of PI-3-COF, named PI-3-COF-lp (low porosity) and PI-3-COF-hp (high porosity) in the following, depending on the selected drying procedure (see SI for details). Fourier transform infrared (FT-IR) spectra of the yellow powdered materials indicate the successful condensation to the imine-linked frameworks, represented by the imine bond vibration ($\nu_{C=N}$) at 1630 cm^{-1} (Figure S 2). The spectra for both samples appear essentially indistinguishable due to their identical chemical composition. Structural analysis by X-ray powder diffraction (XRPD) with Co-K$_{\alpha 1}$ radiation shows four narrow reflections at 2θ = 6.6°, 11.5°, 13.2°, and 17.8°, indexed as 100, 110, 200, and 120 reflections (space group $P\bar{6}$), and a broad stacking reflection (00l) centered at $2\theta \approx 30$° (Figure S 3, Figure S 4). Bragg peaks in the XRPD pattern (Figure 1b) appear essentially at identical positions for both hp- and lp-

5

materials, but with a reduced full width at half maximum (FWHM) for the hp sample, hinting at a better structural definition and long-range order, i.e. crystallinity, of PI-3-COF-hp compared to its lp derivative. 100, 110 and 200 reflections appear broader, with reduced intensity for PI-3-COF-lp (Figure S 4) and show a slight but visible shift ($\Delta(2\theta) < 0.1°$) to higher angles, reminiscent of, but less pronounced than, a reduction in in-plane coherence and contraction due to drying induced stress.[44] A Pawley refinement (Figure S 3) thus gives slightly reduced unit cell parameters of $a = b = 17.9$ Å and $c = 3.47$ Å for PI-3-COF-lp, compared to $a = b = 18.0$ Å and $c = 3.48$ Å for PI-3-COF-lp. Scanning electron and transmission electron microscopy (SEM/TEM) images show agglomerated polycrystalline spherical particles and a polydisperse distribution of (secondary) particle sizes, approximately centered at ~300 nm in diameter (Figure S 5, Figure S 6) for both samples. Some agglomerates show sizes of multiple µm. The surface of these particles is decorated with stings, consisting of crystallites with average diameters of a few tens of nanometers (Figure S 7, Figure S 8). Nitrogen gas sorption experiments (Figure 1c) show a limited nitrogen uptake for PI-3-COF-lp and reveal BET surface areas of $S_{BET} = 442$ m^2g^{-1} and 1620 m^2g^{-1} and total pore volumes of 0.60 cm^3g^{-1} and 1.1 cm^3g^{-1} for PI-3-COF-lp and hp, respectively (Figure S 9, Figure S 10). Calculated pore size distributions by quenched solid density functional theory (QSDFT) based on a carbon model for cylindrical pores are centered at 1.7 nm for both PI-3-COF-lp and hp (Figure S 9b, Figure S 10b). With respect to the characterization data shown, we find that the difference between lp and hp lies in the extent of crystallinity, i.e. structural definition of the two samples, caused for example by inaccessible pores or disorder in PI-3-COF-lp and is not attributed to a difference in chemical composition. This leads to a reduced

porosity in the case of PI-3-COF-lp compared to PI-3-COF-hp. Based on these findings we envisaged using these samples as a basis for PFG-NMR diffusion experiments to investigate the effect of real structure effects such as crystallinity and porosity on the diffusivity.

Probing Diffusion Experimentally by PFG NMR

Due to its abundant use as an organic solvent in synthesis and its sufficiently long T_2 relaxation time (s.b., Table S 1), acetonitrile was selected as a proxy to probe the self-diffusion of molecular reactants or intermediates in the pore system of a COF. Excess amounts of liquid on the outer particle surface or in the interparticle space distort the diffusion experiment and result in a major signal in the ^{1}H-NMR spectrum with bulk liquid-like mobility. To allow for more selective filling of the pores in the materials, we exposed the vacuum-dried materials to saturated acetonitrile vapor in air. Consequently, condensation of acetonitrile into the pores of the material occurred. As indicated by a single, broadened and downfield shifted signal for acetonitrile due to confinement,[45] which is centered at δ = 3.7 ppm in the ^{1}H-NMR spectrum compared to the narrow signal for the isolated liquid at δ = 1.9 ppm (Figure S 15), the liquid mainly condensed into the pores, instead of interparticle voids which would yield signals closer to the free liquid. The mass of the samples increased after this solvent vapor treatment, corresponding to loadings of 25 wt% (PI-3-COF-lp) and 39 wt% (PI-3-COF-hp) of acetonitrile, respectively. Despite these high loadings, the appearance of the loaded materials were identical to the (dry) pristine materials. No liquid was visible on the surface.

PFG-NMR is a useful, non-destructive spectroscopic technique capable of tracking molecular motion and transport on a broad range of distances, varying from nanometers

to hundreds of micrometers. By probing NMR signal attenuations at different diffusion times (Δ), spatial decoding of different diffusion regions and thus, localized as well as long-range information on the structure of porous materials, can be obtained.[46, 47] Fitting of the NMR signal obtained by the pulsed field gradient method using the Stejskal-Tanner[48] equation (Eq. 1) yields the diffusion coefficient (D) as a function of the gradient field strength (g), the gradient pulse duration (δ), and the gyromagnetic ratio of the probed nuclei (γ).

$$I = I_0 \exp\left[-\gamma^2 g^2 \delta^2 \left(\Delta - \frac{\delta}{3}\right) D\right] = I_0 \exp[-BD] \qquad \text{(Eq. 1)}$$

To select appropriate gradient strengths and observation parameters, the relaxation times of the molecules under study are required.[49] Both longitudinal relaxation times ($T_{1,lp}$ = 1.8 s) and transverse relaxation times ($T_{2,lp}$ = 0.54 ms) of acetonitrile loaded onto PI-3-COFs were between one and three orders of magnitude shorter compared to the bulk liquid at 300 K (Table S 1), diagnostic of smaller molecular mobility within the pores.[50] On the one hand, this observation provides further evidence that MeCN is primarily located in the pores of the material, while, on the other hand, short spin-spin relaxation times (T_2) lead to a fast decay of signal intensity in NMR experiments. This sets an experimental upper limit for the gradient pulse duration δ, as well as the diffusion time Δ. Long pulse durations and observation times lead to a bad signal-to-noise ratio, because most of the signal has decayed due to relaxation[49] before the signal can be measured. At the same time, uniform and stable gradients in the spectrometer require a technically limited minimum duration for the gradient pulse, setting the lower limits for δ during a PFG experiment.[46]
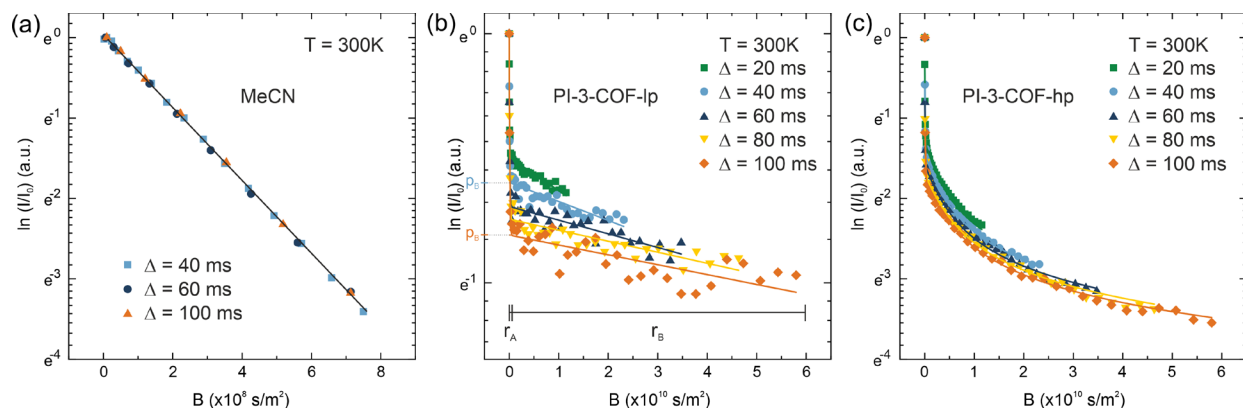
Figure 2: PFG-NMR spin-echo attenuation for (a) liquid MeCN, (b) MeCN loaded PI-3-COF-lp, (c) MeCN loaded PI-3-COF-hp with varying diffusion times (Δ) at T = 300K. Lines represent fits with a mono- or bi-exponential model for MeCN and MeCN loaded COFs, respectively.

For the presented PFG experiments, we chose the minimum technically possible value with our spectrometer of δ = 0.3 ms (at high gradients g_{max} = 900 Gs^{1}cm^{-1}) to acquire PFG spin-echoes for diffusion times Δ = 20–100 ms using a stimulated echo (ste) pulse sequence (see SI for details). As shown in Figure 2, the spin-echo attenuations appear non-linear for both samples, although linearity in the semi-logarithmic representation would be expected for regular isotropic diffusion as observed for bulk acetonitrile (Figure 2a, Figure S 13). The course of the signals can be separated into two regimes: A steeply decreasing initial range for small gradients (r_A) and then a slowly decaying range towards large gradients (r_B) at a fixed pulse duration δ = 0.3 ms. This behavior is characteristic of a distribution of diffusion coefficients, for example observed in porous materials[51] including zeolites[52, 53] and MOFs,[54] where regions with different translational mobilities are found. This behavior can be observed in these materials for example for molecules diffusing inside versus outside of crystallites.[55] A bi-exponential model (Eq. 2) can fit attenuations with this behavior, where p_i reflects the population of the region (i) with diffusivity D_i.[51, 56] The diffusivities of both regions appear as linear ranges in the semi-logarithmic plot.

$$\frac{I}{I_0} = p_A \exp[-BD_A] + p_B \exp[-BD_B]$$ (Eq. 2)

The observed signal attenuations in PI-3-COF-lp (b) are in good agreement with this simple bi-exponential model. For varying diffusion times, different slopes are visible in the range r_B towards high gradients (Figure 2b), indicating a dependence of the diffusivity D_B on diffusion time Δ. With variation of Δ also the population p_i, which can be interpreted as the y-intercept of the linear, slowly decaying intensity extrapolated to $B = 0$ (Figure 2b), changes. The population p_B decreases with longer observation times (Figure 2b). This phenomenon indicates a molecular exchange between both regions in the material, expected for open pore channels in PI-3-COF, and can be used by the NMR tracer exchange method[57] to determine the fraction of molecules and their mean lifetime τ_i within these regions.[58, 59] With a defined macroscopic particle geometry, e.g. in single crystals, or for spherical particles, their diffusivity and average lifetime allows to estimate mean particle/crystallite sizes.[54, 60, 61] Unfortunately, the wide distribution of particles sizes and shapes in our materials, as observed by electron microscopy (Figure S 5, Figure S 6) does not allow for this analysis. Applying the simple bi-exponential model to PI-3-COF-lp yields two diffusion coefficients of D_A = 1.7 × 10^{-8} m^{2}s^{-1} and D_B = 1.4 × 10^{-11} m^{2}s^{-1}, with Δ = 20 ms at T = 300 K. A comparison of the exchange behavior between these regions at reduced temperature down to T = 280 K shows that the population p_A drops at reduced temperatures and the exchange between both regions becomes less prominent (Figure S 16). Analysis of the population p_B at temperatures between T = 300 K and T = 280 K as a function of Δ further corroborates this finding, evident from a slower decrease of p_B vs. Δ at reduced temperature (Figure S 18). The

10

diffusivity D_A = 1.7 × 10^{-8} m^{2}s^{-1} exceeds the self-diffusion coefficient of pure acetonitrile (D_s = 4.5 × 10^{-9} m^{2}s^{-1}, Figure S 14) at T = 300 K by one order of magnitude. The high diffusivity and strong temperature dependence of p_B (Figure S 18) suggest that D_A corresponds to an averaged diffusion of liquid acetonitrile molecules, which exchanged with the gas phase during the time of the NMR experiment.[62, 63] With reduced temperature, the vapor pressure of acetonitrile and thus the partial pressure of MeCN in the gas phase, as well as the probability for a phase exchange during the observation time, is reduced. Contrary to p_A, we conclude that the molecules of the population p_B have not exchanged with the gas phase during the time of the NMR experiment, and can be labeled as the fraction of molecules remaining within the particle. Their diffusivity D_B thus denotes intraparticle diffusion of acetonitrile within the pore channels of the polycrystalline particles of PI-3-COF. A comparison of D_B at constant temperature (Figure S 19) shows a decrease of D_B with increasing diffusion times Δ. In contrast to this, diffusion in the non-confined, isotropic bulk-liquid is independent of Δ (Figure 2a, Figure S 13). Similar to observations in lithium ion conductors[64] and polycrystalline faujasite crystals,[65] long-range diffusion of MeCN in PI-3-COF-lp, corresponding to long diffusion times Δ, is limited by transport barriers (e.g. grain boundaries or surface effects[52, 66]), whereas at small displacements these defects have less effect on the diffusion coefficient.[52] To solely observe intracrystalline diffusion and reduce the influence of intercrystallite or interparticle diffusion resistances, D_B should ideally be measured at short diffusion times, where the mean square displacements ($\langle z^2 \rangle \approx 2D\Delta$) for most diffusing molecules in this time interval are smaller than the average crystallite diameter. However, due to technical limitations, Δ cannot be chosen arbitrarily small for high gradient values.[46] Because the accessible

isotropic diffusion lengths in the presented materials (μm range, Table S 2) exceed the observed crystallite size of a few tens of nanometers by SEM/TEM analysis (s. a.), only effective long-range diffusion coefficients can be obtained from the experiments. To estimate the order of magnitude for short-range diffusion in the pores of PI-3-COF, we extrapolated the experimental values for D_B towards short diffusion times in a phenomenological log(D)-log(Δ) plot, which has been used to describe for example restricted diffusion in zeolites (Figure S 20).[52] The extrapolation suggests that D_B may approach values up to the order of 10^{-10} $m^2 s^{-1}$ for PI-3-COF-lp. The extrapolated values, however, should be interpreted with care as they might overestimate short-range diffusivity: The experimental diffusion coefficients for D_B may still contain a contribution of a fraction of acetonitrile diffusing in textural mesopores or small voids between individual crystallites, which would give rise to more bulk-like diffusivities. The presence of such textural pores can be inferred from acetonitrile vapor sorption experiments with PI-3-COF-lp (Figure S 11): The vapor sorption isotherm at 300 K shows a steep uptake at low relative pressures (P/P$_{sat}$ < 0.13), corresponding to the filling of micropores, i.e. pore channels (structural pores). Towards higher relative pressure, a further but less steep uptake with pronounced hysteresis is visible. This uptake is attributed to the filling of textural mesopores. In turn, we conclude that some signal intensity during the NMR experiments may be caused by acetonitrile molecules in small textural pores, besides those in structural pores (pore channels of PI-3-COF). In addition, the linearity of the signal corresponding to intraparticle mobility D_B (Figure 2) as well as the absence of additional signals during relaxation experiments suggests that the obtained PFG attenuation is not amenable to further quantitative differentiation of structural and textural

pores. Relaxation times (Table S 1) as well as diffusion coefficients of molecules in these different pore regimes may appear superimposed and thus indistinguishable, likely influenced by a fast exchange between them relative to the NMR experiment timescale. The PFG NMR signal attenuation curves for MeCN loaded PI-3-COF-hp (Figure 2b) similarly show two separated ranges and exchange between the corresponding regions, evident from an offset of the slowly decaying range (r_B). In contrast to PI-3-COF-lp, however, the signal attenuation appears to be non-linear. This phenomenon indicates a contribution of anisotropic diffusion, which is in line with a diffusion along the 1D pore channels of PI-3-COF. Similar attenuations have been observed for anisotropic diffusion in pore channels of aluminum fumarate MOFs[55, 67] and mesoporous silica SBA-15.[68] To address this effect of anisotropy to the observed PFG signal attenuation, the second term of the simple bi-exponential model was adjusted to a previously developed anisotropic model for hierarchically porous SBA-15 catalysts (Eq. 3).[69] Notably, this model uses a simplified approximation to account for the molecular exchange between the different regions (p_A and p_{aniso}) in the material, based on the more complex solution developed by Spith *et. al.*[55], which requires a negligibly small population p_A of the region with isotropic diffusion. Similar to the assumptions for the hierarchically ordered SBA-15 materials, however, we need to consider a fraction of MeCN present in small textural pores at the respective loadings of MeCN in the PI-3-COF samples under study, which is in contrast to the boundary conditions of the model by Spith *et. al.*

$$\frac{I}{I_0} \approx p_A \exp[-BD_A] + p_{aniso} \exp[-BD_{perp}] \left[\frac{\sqrt{\pi}}{2} \frac{\mathrm{erf}\{\sqrt{B(D_{par} - D_{perp})}\}}{\sqrt{B(D_{par} - D_{perp})}} \right] \qquad \text{(Eq. 3)}$$

Applying Eq. 3 to the observed signal attenuations for PI-3-COF-hp gives an isotropic diffusion coefficient D_A, and two different anisotropic diffusion coefficients for movement of molecules parallel (D_{par}) and perpendicular (D_{perp}) to the channel direction. The fit shows excellent agreement with experimental data (Figure 2c) and yields two diffusion coefficients of D_A = 2.2 × 10^{-8} m^{2}s^{-1} and D_{par} = 6.1 × 10^{-10} m^{2}s^{-1}, with Δ = 20 ms at T = 300 K and $D_{perp} \rightarrow$ 0, which is in-line with the structural model of PI-3-COF consisting of closely stacked 2D layers that restrict diffusion between the layers, e.g. perpendicular to the channel direction. Analogous to the exchange behavior observed for PI-3-COF-lp, the material shows temperature-dependent molecular exchange between both regions, with D_A comprising contributions of gas diffusion through gas-liquid exchange during the observation time (Figure S 17). Extrapolation of the experimental values for D_{par} in the log(D)-log(Δ) plot[52] gives values up to the order of 10^{-9} m^{2}s^{-1}, similar to diffusion in the bulk liquid, towards short diffusion times. In summary, diffusion in the high porosity sample is less affected by defects or limited pore accessibility, resulting in an observable anisotropic diffusion parallel to the channel direction that is on average one to two orders of magnitude faster compared to PI-3-COF-lp.
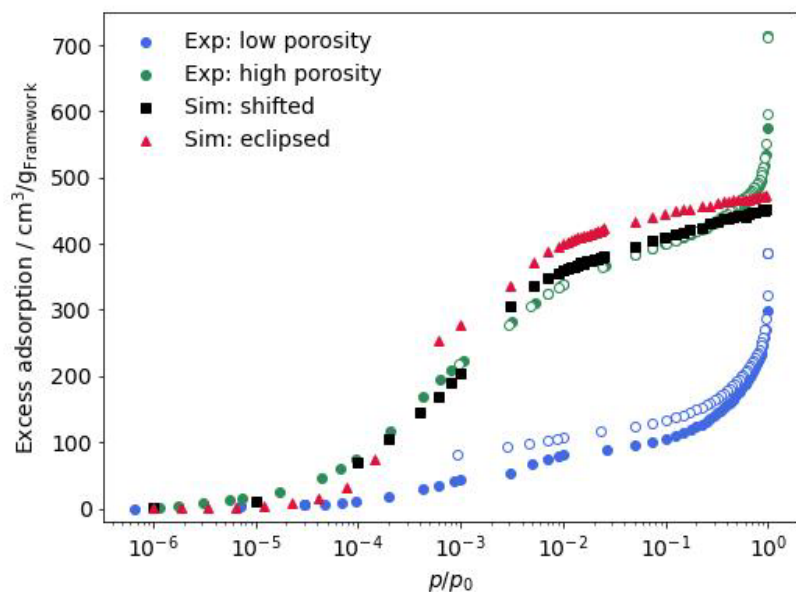
Figure 3 Comparison between experimental N$_2$ adsorption isotherms at 77K (low porosity in blue, high porosity in green) and simulated ones. The isotherm resulting from the shifted structure is depicted in black squares, the one of the eclipsed stacked structure in red triangles.

Following previous work[70] the structural model obtained from X-ray powder diffraction experiments was refined by density functional calculations under periodic boundary conditions as described in more detail in the Supporting Information. Figure 3 shows simulated and experimental excess nitrogen adsorption isotherms for PI-3-COF. The two experimental curves correspond to the lp and hp samples while the two simulated curves correspond to a model structure in which the layers are perfectly eclipsed (red triangles) and one model structure in which two adjacent layers are slightly shifted by approx. 1.7 Å in an alternating way (black squares) such that the first and the third layer as well as the second and the fourth layer and so on are eclipsed. This model mimics the effect of offset layer stacking, often found in COFs for example as layer displacement in randomized

directions.[70-74] In both cases the interlayer distance was fixed to a value of 3.65 Å resulting from the DFT optimization for the shifted structure. The two structures are visualized in Figure 4. The good agreement between the simulated isotherms and the experimental curve of the hp sample indicates a high degree of crystallinity and accessibility of the experimental sample. In contrast to our previous work,[70] no scaling factor was required to account for the finding that the simulation usually overestimated the experimental isotherm. The divergence of the experimental isotherms close to the saturation pressure results from condensation of nitrogen in textural macropores and is therefore not captured in the simulation, which is based on an infinite ideal structure. As found previously,[70] the isotherm corresponding to the shifted structure shows a smoother increase in loading with increasing pressure compared to the eclipsed structure. Given the qualitative difference between the two simulated isotherms in the medium pressure range between $p/p_0 = 10^{-4}$ and 10^{-2} despite rather small structural differences in the two model COFs, the good agreement between experiment and simulation for the artificial, idealized structural model over the entire pressure range is remarkable and suggests that the real structure in the material is characterized by small shifts between the different layers.
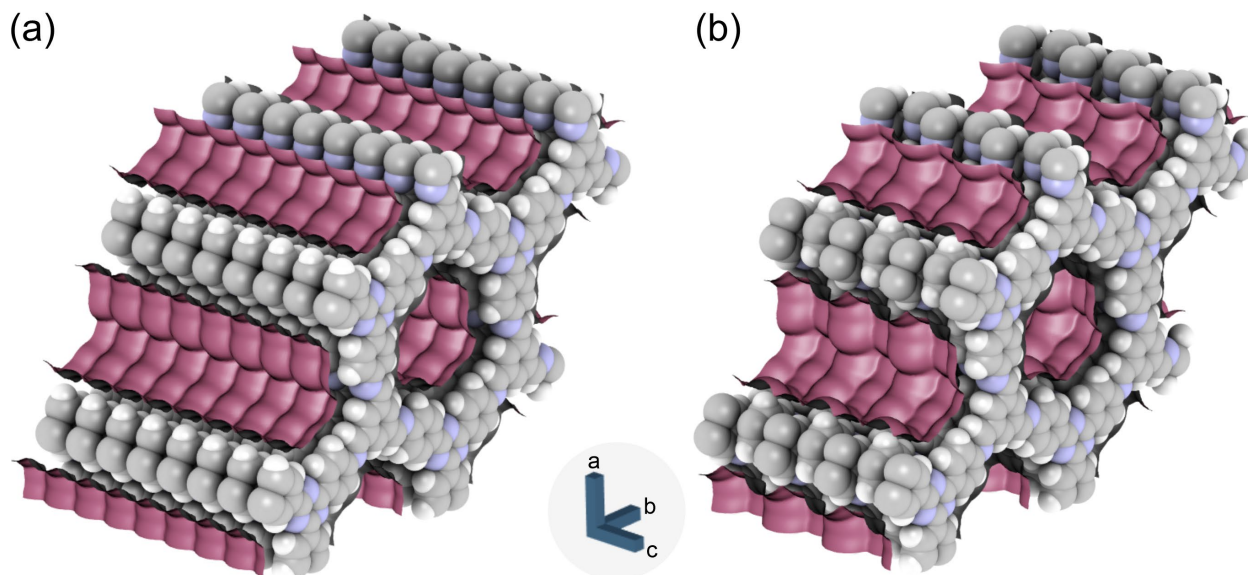
(a)   (b)

Figure 4 Visualization of the eclipsed (a) and the shifted structure (b) of PI 3-COF. Violet surfaces depict the N_2 accessible pore surface based on Van der Waals parameters.

The self-diffusion coefficient of acetonitrile in the two structures at 300 K amounts to 1.02×10^{-9} m^2s^{-1} in the perfectly eclipsed structure and to 0.70×10^{-9} m^2s^{-1} in the shifted structure, which corresponds to a reduction by a factor of 3.7 and 5.4, respectively, compared to the bulk liquid value of 3.76×10^{-9} m^2s^{-1} at 298 K, predicted by the molecular model. This bulk value is close to the experimentally determined self-diffusion coefficients reported in the literature ($D \approx 4.2 \times 10^{-9}$ m^2s^{-1})[75, 76] and measured in the present study ($D \approx 4.5 \times 10^{-9}$ m^2s^{-1}). However, since the simulated value of bulk diffusion does not exactly match the experiment, it is reasonable to compare the ratios of the bulk and pore diffusion coefficients in addition to the absolute values. The ratio between the diffusion coefficients of liquid MeCN in bulk (this study) vs. PI-3-COF-hp (PFG) of 7.4 obtained in the present work is in good agreement with the ratio of 5.4 for the bulk value vs. the simulation result for the shifted structure at 300 K.

In other simulation works ratios of 2.0 and 3.2 were reported for diffusion of MeCN in a carbon nanotube of 1.5 nm diameter[77] and an amorphous silica sample of 2.4 nm

17

diameter[78], respectively. Experimental studies reporting the self-diffusion of acetonitrile under confinement show a diverse picture. In pores smaller than 1 nm self-diffusion coefficients on the order of 10^{-11} m^2s^{-1} were measured for zeolite NaX[58] and porous carbon[79], respectively. In a sol-gel glass with a reported diameter of 2.9 nm a diffusion coefficient of 1.1×10^{-9} m^2s^{-1} was obtained[80], i.e. similar to the diffusion coefficient reported for a mesoporous MCM-41 sample (pore size 3.6 nm, D = 9.9×10^{-10} m^2s^{-1})[81] and larger than the diffusion coefficient reported for a porous carbon (pore size 4.8 nm, D = 6.0×10^{-10} m^2s^{-1})[79]. Experiments probing a pore size similar to the one in the present work are scarce. For a MCM-41 sample with a pore size of 2 nm a diffusion coefficient of 2.7×10^{-10} m^2s^{-1} was reported[81], which is relatively close to the value obtained for the hp sample in the present work. We note that not only the pore diameter affects the self-diffusion coefficient under confinement but also the interactions of the diffusing compound with the pore wall, in particular for narrow pores. Therefore, the comparison with other materials can only provide a qualitative picture.

Discussion

The present work aims at clarifying the comparability of the self-diffusion coefficient of acetonitrile in a covalent organic framework obtained from MD simulations and PFG NMR measurements. For this purpose, two model structures were investigated in conjunction with a fluid model that captures the bulk diffusion coefficient reasonably well. The theoretical model, applied to ideal structural models of isolated pore channels, suggests a comparably fast diffusion within the structural pore channels of PI-3-COF in both fully eclipsed and offset stacked cases, albeit with slightly reduced diffusivity in the offset stacked case. The obtained simulated diffusion coefficients are slightly lower, yet roughly

18

of the same order of magnitude as isotropic diffusion in the bulk liquid. We complemented our simulation studies with experimental data obtained by PFG NMR experiments. We observed short T_2 relaxation times for the confined liquid in the pores of PI-3-COF. This limits diffusion times and pulse durations applicable during PFG experiments. Due to the limited crystallite sizes in the polycrystalline COF particles, the experimentally observed diffusion coefficients were limited to mid-to-long range diffusion processes across multiple crystallites, given the technical limits for short pulse durations at high gradient strengths. By deconvolution of the obtained NMR signal attenuation, we identified multicomponent diffusion with open pore channels allowing the equilibrium exchange of molecules between the surrounding vapor phase and pore liquid. PFG measurements at reduced temperature helped to assign these contributions by limiting the gas-liquid exchange. The experimental diffusivity in PI-3-COF samples was obtained as effective diffusion coefficients and found to decrease for long diffusion times. This behavior points at real structure effects, e.g. defects and surface barriers at crystal boundaries within and between the particles.[65, 82] For a sample of PI-3-COF with lower porosity these effects are more dominant compared to the sample with higher porosity, and led to the observation of effective diffusivities on the order of 10^{-11} m^{2}s^{-1} and 10^{-10} m^{2}s^{-1} for lp and hp samples, respectively. Extrapolation of the obtained diffusivities toward short diffusion times, i.e. small mean square displacements, indicate that short-range diffusion may be one (hp) to two orders (lp) of magnitude faster than the observable long-range diffusion. The high porosity sample of PI-3-COF showed anisotropy in diffusion, characterized by diffusivities which agree well with the simulated values for the offset stacked model, both being in the order of 10^{-10} m^{2}s^{-1}. In contrast, the reduced structural definition of the lp

sample led to the observation of isotropic diffusion only. This observation hints at the dominant influence of diffusion barriers in the material, restricting the diffusion of acetonitrile to shorter displacements and reducing its mobility compared to the hp sample. Thus, we point out that limited structural order not only reduces the accessible pore volume, i.e. porosity, but also restricts the mobility of molecules *via* diffusion barriers. As these are essentially invisible to typical analytical techniques, including gas sorption experiments, PFG NMR spectroscopy should be considered as a complementary method to assess diffusivity-dependent parameters, such as turnover frequency or selectivity of reactions with COFs as heterogeneous catalysts.

Comparing the experimental to the simulated results helps to pinpoint important insights into the real structure of the material. Our comparison between calculated nitrogen gas adsorption isotherms for eclipsed und offset structures in a pressure range $p/p_0 = 10^{-4}$ and 10^{-2} shows profound sensitivity for localized differences in the stacking and suggests small displacements of the layers in the material, since the experimentally observed isotherm of PI-3-COF-hp closely resembles the simulated isotherms of the offset stacked structure with remarkable agreement. Thus, simulated isotherms may serve as a handle to pinpoint local characteristics in the real structure of the material, although these simulations are generally based on artificial, idealized structural models.

Conclusion

The combined experiments and simulations shine light on prevalent diffusion mechanisms and issues associated with the experimental determination of diffusion coefficients in covalent organic frameworks. However, the direct observation of pure short-range, i.e. undisturbed intracrystalline diffusion within the pore channels, requires

large (ideally single crystalline) particles with pore channel lengths in the µm range. Most powdered COF materials obtained from typical synthetic procedures do not meet this requirement, and obtaining crystallite sizes in this range is a rarely tackled and challenging task for imine and other COFs.[83] Nevertheless, our systematic computational and experimental study sets the stage for future exploration of diffusion processes in covalent organic frameworks and related systems. We propose that optimizing the synthesis conditions to obtain domain sizes in the µm range should be the basis for future studies. With these requirements in mind, we expect that the influence of pore sizes and the chemical structure of the pore walls as well as their surface polarity, and the impact of meso/macro porosity on diffusion processes become experimentally accessible.

Data Availability Statement

Discussions of methods and equipment used, synthetic procedures, FT-IR spectra, XRPD data and structure refinements, (pulsed field gradient) ^{1}H NMR spectra, nitrogen gas sorption isotherms, pore-size distributions, BET plots, acetonitrile vapor adsorption isotherms can be found in the Supporting Information file. Additional material, cif files, RASPA and Gromacs input files and a Jupyter notebook containing the analysis can be retrieved from the Data Repository of the University of Stuttgart (DaRUS) under https://doi.org/10.18419/darus-3269.

Information for Review only

During the review process the repository can be accessed via the private URL https://darus.uni-stuttgart.de/dataset.xhtml?persistentId=doi%3A10.18419%2Fdarus-3269&version=DRAFT.

Acknowledgments

Author Contributions

L.G. synthesized and analyzed the materials and precursors, performed PFG-NMR diffusion experiments and interpreted experimental data. C.K. performed GCMC and MD simulations with support by T.W.T. R.S. performed DFT calculations. F.H. performed gas and vapor sorption experiments. L.G. wrote the manuscript with input from C.K. and N.H. J.K., J.G., B.V.L. and N.H. supervised the research. All authors read and commented on the manuscript.

ORCID

Lars Grunenberg: 0000-0002-6831-4626

Christopher Keßler: 0000-0003-0928-5041

Tiong Wei Teh: 0009-0005-5218-2277

Robin Schuldt: 0000-0001-5743-4561

Fabian Heck: 0000-0003-0198-3398

Johannes Kästner: 0000-0001-6178-7669

Joachim Groß: 0000-0001-8632-357X

Bettina V. Lotsch: 0000-0002-3094-303X

Niels Hansen: 0000-0003-4366-6120

Competing Interests Statement

The authors declare no competing financial interests.

References

1. Keller N., Bein T. Optoelectronic Processes in Covalent Organic Frameworks. *Chem. Soc. Rev.* **50**, 1813-1845 (2021).
2. Lohse M. S., Bein T. Covalent Organic Frameworks: Structures, Synthesis, and Applications. *Adv. Funct. Mater.* **28** (2018).
3. Lyu H. et al. Covalent Organic Frameworks for Carbon Dioxide Capture from Air. *J. Am. Chem. Soc.* **144**, 12989-12995 (2022).
4. Xu F. et al. Energy-Storage Covalent Organic Frameworks: Improving Performance Via Engineering Polysulfide Chains on Walls. *Chem. Sci.* **10**, 6001-6006 (2019).
5. Xu F. et al. Radical Covalent Organic Frameworks: A General Strategy to Immobilize Open-Accessible Polyradicals for High-Performance Capacitive Energy Storage. *Angew. Chem. Int. Ed.* **54**, 6814-6818 (2015).
6. Furukawa H., Yaghi O. M. Storage of Hydrogen, Methane, and Carbon Dioxide in Highly Porous Covalent Organic Frameworks for Clean Energy Applications. *J. Am. Chem. Soc.* **131**, 8875-8883 (2009).

7. Diercks C. S. et al. Reticular Electronic Tuning of Porphyrin Active Sites in Covalent Organic Frameworks for Electrocatalytic Carbon Dioxide Reduction. *J. Am. Chem. Soc.* **140**, 1116-1122 (2018).

8. Wang X. et al. Sulfone-Containing Covalent Organic Frameworks for Photocatalytic Hydrogen Evolution from Water. *Nat. Chem.* **10**, 1180-1189 (2018).

9. Biswal B. P. et al. Sustained Solar H(2) Evolution from a Thiazolo[5,4-D]Thiazole-Bridged Covalent Organic Framework and Nickel-Thiolate Cluster in Water. *J. Am. Chem. Soc.* **141**, 11082-11092 (2019).

10. Mitschke B., Turberg M., List B. Confinement as a Unifying Element in Selective Catalysis. *Chem* **6**, 2515-2532 (2020).

11. Tan K. T., Tao S., Huang N., Jiang D. Water Cluster in Hydrophobic Crystalline Porous Covalent Organic Frameworks. *Nat. Commun.* **12**, 6747 (2021).

12. Zeng W. J. et al. Covalent Organic Frameworks as Micro-Reactors: Confinement-Enhanced Electrochemiluminescence. *Chem. Sci.* **11**, 5410-5414 (2020).

13. Zhao J. et al. A "One-Step" Approach to the Highly Efficient Synthesis of Lactide through the Confinement Catalysis of Covalent Organic Frameworks. *Green Chem.* **25**, 3103-3110 (2023).

14. Emmerling S. T. et al. Olefin Metathesis in Confinement: Towards Covalent Organic Framework Scaffolds for Increased Macrocyclization Selectivity. *Chemistry* **28**, e202104108 (2022).

15. Gao W. Y., Cardenal A. D., Wang C. H., Powers D. C. In Operando Analysis of Diffusion in Porous Metal-Organic Framework Catalysts. *Chem. Eur. J.* **25**, 3465-3476 (2019).

16. Fang Q. et al. 3d Microporous Base-Functionalized Covalent Organic Frameworks for Size-Selective Catalysis. *Angew. Chem. Int. Ed.* **53**, 2878-2882 (2014).

17. North A. M. Diffusion-Controlled Reactions. *Q. Rev. Chem. Soc.* **20**, 421 (1966).

18. Shinde D. B. et al. Crystalline 2d Covalent Organic Framework Membranes for High-Flux Organic Solvent Nanofiltration. *J. Am. Chem. Soc.* **140**, 14342-14349 (2018).

19. Shi X. et al. Design of Three-Dimensional Covalent Organic Framework Membranes for Fast and Robust Organic Solvent Nanofiltration. *Angew. Chem. Int. Ed.* **61**, e202207559 (2022).

20. Karak S., Dey K., Banerjee R. Maneuvering Applications of Covalent Organic Frameworks Via Framework-Morphology Modulation. *Adv. Mater.* **34**, e2202751 (2022).

21. Wang R., Guo J., Xue J., Wang H. Covalent Organic Framework Membranes for Efficient Chemicals Separation. *Small Struct.* **2**, 2100061 (2021).

22. Yang Y. et al. Constructing Chemical Stable 4-Carboxyl-Quinoline Linked Covalent Organic Frameworks Via Doebner Reaction for Nanofiltration. *Nat. Commun.* **13**, 2615 (2022).

23. Krishna R. Describing the Diffusion of Guest Molecules inside Porous Structures. *J. Phys. Chem. C* **113**, 19756-19781 (2009).

24. Jakobtorweihen S. et al. Understanding the Loading Dependence of Self-Diffusion in Carbon Nanotubes. *Phys. Rev. Lett.* **95**, 044501 (2005).

25. Obliger A., Bousige C., Coasne B., Leyssale J.-M. Development of Atomistic Kerogen Models and Their Applications for Gas Adsorption and Diffusion: A Mini-Review. *Energy Fuels* **37**, 1678-1698 (2023).

26. Dubbeldam D., Snurr R. Q. Recent Developments in the Molecular Modeling of Diffusion in Nanoporous Materials. *Mol. Simul.* **33**, 305-325 (2007).

27. Jobic H., Theodorou D. N. Quasi-Elastic Neutron Scattering and Molecular Dynamics Simulation as Complementary Techniques for Studying Diffusion in Zeolites. *Microporous Mesoporous Mater.* **102**, 21-50 (2007).

28. Demontis P., Suffritti G. B. Structure and Dynamics of Zeolites Investigated by Molecular Dynamics. *Chem. Rev.* **97**, 2845-2878 (1997).

29. Sholl D. S. Understanding Macroscopic Diffusion of Adsorbed Molecules in Crystalline Nanoporous Materials Via Atomistic Simulations. *Acc. Chem. Res.* **39**, 403-411 (2006).

30. Smit B., Maesen T. L. Molecular Simulations of Zeolites: Adsorption, Diffusion, and Shape Selectivity. *Chem. Rev.* **108**, 4125-4184 (2008).

31. Skoulidas A. I. Molecular Dynamics Simulations of Gas Diffusion in Metal-Organic Frameworks: Argon in Cubtc. *J. Am. Chem. Soc.* **126**, 1356-1357 (2004).

32. Skoulidas A. I., Sholl D. S. Self-Diffusion and Transport Diffusion of Light Gases in Metal-Organic Framework Materials Assessed Using Molecular Dynamics Simulations. *J. Phys. Chem. B* **109**, 15760-15768 (2005).

33. Yang Q., Zhong C. Molecular Simulation of Adsorption and Diffusion of Hydrogen in Metal-Organic Frameworks. *J. Phys. Chem. B* **109**, 11862-11864 (2005).

34. Düren T., Snurr R. Q. Assessment of Isoreticular Metal−Organic Frameworks for Adsorption Separations: A Molecular Simulation Study of Methane/N-Butane Mixtures. *J. Phys. Chem. B* **108**, 15703-15708 (2004).

35. Garberoglio G., Vallauri R. Adsorption and Diffusion of Hydrogen and Methane in 2d Covalent Organic Frameworks. *Microporous Mesoporous Mater.* **116**, 540-547 (2008).

36. Keskin S. Adsorption, Diffusion, and Separation of CH_4/H_2 Mixtures in Covalent Organic Frameworks: Molecular Simulations and Theoretical Predictions. *J. Phys. Chem. C* **116**, 1772-1779 (2012).

37. Yang Z., Cao D. Effect of Li Doping on Diffusion and Separation of Hydrogen and Methane in Covalent Organic Frameworks. *J. Phys. Chem. C* **116**, 12591-12598 (2012).

38. Zeng H., Liu Y., Liu H. Adsorption and Diffusion of CO_2 and CH_4 in Covalent Organic Frameworks: An Mc/Md Simulation Study. *Mol. Simul.* **44**, 1244-1251 (2018).

39. Altundal O. F., Haslak Z. P., Keskin S. Combined GCMC, MD, and DFT Approach for Unlocking the Performances of Cofs for Methane Purification. *Ind. Eng. Chem. Res.* **60**, 12999-13012 (2021).

40. Bukowski B. C. et al. Connecting Theory and Simulation with Experiment for the Study of Diffusion in Nanoporous Solids. *Adsorption* **27**, 683-760 (2021).

41. Ford D. C. et al. Self-Diffusion of Chain Molecules in the Metal-Organic Framework Irmof-1: Simulation and Experiment. *J. Phys. Chem. Lett.* **3**, 930-933 (2012).

42.   Dutta S. et al. Molecular Diffusion in Hierarchical Zeolites with Ordered Mesoporosity: Pulsed Field Gradient Nuclear Magnetic Resonance Combined with Thermodynamic Modeling. *J. Phys. Chem. C* **127**, 1548-1559 (2023).

43.   Grunenberg L. et al. Amine-Linked Covalent Organic Frameworks as a Platform for Postsynthetic Structure Interconversion and Pore-Wall Modification. *J. Am. Chem. Soc.* **143**, 3430-3438 (2021).

44.   Grunenberg L. et al. Postsynthetic Transformation of Imine- into Nitrone-Linked Covalent Organic Frameworks for Atmospheric Water Harvesting at Decreased Humidity. *J. Am. Chem. Soc.* **145**, 13241-13248 (2023).

45.   Das A. et al. Single-File Diffusion of Confined Water inside SWNTs: An NMR Study. *ACS Nano* **4**, 1687-1695 (2010).

46.   Kärger J. et al. Pulsed Field Gradient NMR Diffusion Measurement in Nanoporous Materials. *Adsorption* **27**, 453-484 (2021).

47.   Kärger J., Chmelik C., Heinke L., Valiullin R. A New View of Diffusion in Nanoporous Materials. *Chem. Ing. Tech.* **82**, 779-804 (2010).

48.   Tanner J. E. Use of the Stimulated Echo in NMR Diffusion Studies. *J. Chem. Phys.* **52**, 2523-2526 (1970).

49.   Kärger J., Pfeifer H., Heink W. Principles and Application of Self-Diffusion Measurements by Nuclear Magnetic Resonance. In: Waugh JS (ed). *Advances in Magnetic and Optical Resonance*, vol. 12. Academic Press, 1988, pp 1-89.

50.   Hertel S. et al. NMR Studies of Benzene Mobility in Metal-Organic Framework Mof-5. *The European Physical Journal Applied Physics* **55** (2011).

51.   Valiullin R. R., Skirda V. D., Stapf S., Kimmich R. Molecular Exchange Processes in Partially Filled Porous Glass as Seen with NMR Diffusometry. *Phys. Rev. E* **55**, 2664-2671 (1997).

52.   Hedin N. et al. Intracrystalline Transport Barriers Affecting the Self-Diffusion of Ch(4) in Zeolites |Na(12)|-a and |Na(12-X)K(X)|-A. *Langmuir* **35**, 12971-12978 (2019).

53.   Morgan M., Cosgrove T., Richardson R. The Diffusion of Benzene in High Silica Zeolite Zsm5 Studied by PFGNMR and Quens. *Colloids Surf.* **36**, 209-219 (1989).

54.   Stallmach F. et al. NMR Studies on the Diffusion of Hydrocarbons on the Metal-Organic Framework Material Mof-5. *Angew. Chem. Int. Ed.* **45**, 2123-2126 (2006).

55.   Splith T., Frohlich D., Henninger S. K., Stallmach F. Development and Application of an Exchange Model for Anisotropic Water Diffusion in the Microporous Mof Aluminum Fumarate. *J. Magn. Reson.* **291**, 40-46 (2018).

56.   Kärger J. Zur Bestimmung Der Diffusion in Einem Zweibereichsystem Mit Hilfe Von Gepulsten Feldgradienten. *Ann. Phys,* **479**, 1-4 (1969).

57.   Kärger J. A Study of Fast Tracer Desorption in Molecular Sieve Crystals. *AIChE J.* **28**, 417-423 (1982).

58.   Kärger J., Pfeifer H. N.M.R. Self-Diffusion Studies in Zeolite Science and Technology. *Zeolites* **7**, 90-107 (1987).

59.   Zeigermann P. et al. Diffusion in Hierarchical Mesoporous Materials: Applicability and Generalization of the Fast-Exchange Diffusion Model. *Langmuir* **28**, 3621-3632 (2012).

60. Loskutov V. V., Sevriugin V. A. A Novel Approach to Interpretation of the Time-Dependent Self-Diffusion Coefficient as a Probe of Porous Media Geometry. *J. Magn. Reson.* **230**, 1-9 (2013).

61. Latour L. L., Mitra P. P., Kleinberg R. L., Sotak C. H. Time-Dependent Diffusion Coefficient of Fluids in Porous Media as a Probe of Surface-to-Volume Ratio. *J. Magn. Reson.* **101**, 342-346 (1993).

62. Forse A. C. et al. Influence of Pore Size on Carbon Dioxide Diffusion in Two Isoreticular Metal–Organic Frameworks. *Chem. Mater.* **32**, 3570-3576 (2020).

63. Vasenkov S., Geir O., Karger J. Gas Diffusion in Zeolite Beds: PFG NMR Evidence for Different Tortuosity Factors in the Knudsen and Bulk Regimes. *Eur Phys J E Soft Matter* **12 Suppl 1**, S35-38 (2003).

64. Holzmann T. et al. Li0.6[Li0.2sn0.8s2] – a Layered Lithium Superionic Conductor. *Energy & Environmental Science* **9**, 2578-2585 (2016).

65. Beckert S. et al. Tracing Water and Cation Diffusion in Hydrated Zeolites of Type Li-Lsx by Pulsed Field Gradient NMR. *J. Phys. Chem. C* **117**, 24866-24872 (2013).

66. Krutyeva M. et al. Surface Barriers on Nanoporous Particles: A New Method of Their Quantitation by PFG NMR. *Microporous Mesoporous Mater.* **104**, 89-96 (2007).

67. Peksa M., Lang J., Stallmach F. 13C NMR Study of Diffusion Anisotropy of Carbon Dioxide Adsorbed in Nanoporous DMOF-1. *Microporous Mesoporous Mater.* **205**, 11-15 (2015).

68. Naumov S. et al. Tracing Pore Connectivity and Architecture in Nanostructured Silica Sba-15. *Microporous Mesoporous Mater.* **110**, 37-40 (2008).

69. Isaacs M. A. et al. Unravelling Mass Transport in Hierarchically Porous Catalysts. *J. Mater. Chem. A* **7**, 11814-11825 (2019).

70. Kessler C. et al. Influence of Layer Slipping on Adsorption of Light Gases in Covalent Organic Frameworks: A Combined Experimental and Computational Study. *Microporous Mesoporous Mater.* **336**, 111796 (2022).

71. Pütz A. M. et al. Total Scattering Reveals the Hidden Stacking Disorder in a 2d Covalent Organic Framework. *Chem. Sci.* **11**, 12647-12654 (2020).

72. Haase F. et al. Tuning the Stacking Behaviour of a 2d Covalent Organic Framework through Non-Covalent Interactions. *Mater. Chem. Front.* **1**, 1354-1361 (2017).

73. Emmerling S. T. et al. Interlayer Interactions as Design Tool for Large-Pore Cofs. *J. Am. Chem. Soc.* **143**, 15711-15722 (2021).

74. Stahler C. et al. Light-Driven Molecular Motors Embedded in Covalent Organic Frameworks. *Chem. Sci.* **13**, 8253-8264 (2022).

75. Viel S. et al. Pulsed Field Gradient Magic Angle Spinning NMR Self-Diffusion Measurements in Liquids. *J. Magn. Reson.* **190**, 113-123 (2008).

76. Cohen S. R. et al. Structure and Dynamics of Acetonitrile: Molecular Simulation and Neutron Scattering. *J. Mol. Liq.* **348**, 118423 (2022).

77. Kalugin O. N., Chaban V. V., Loskutov V. V., Prezhdo O. V. Uniform Diffusion of Acetonitrile inside Carbon Nanotubes Favors Supercapacitor Performance. *Nano Lett.* **8**, 2126-2130 (2008).

78. Norton C. D., Thompson W. H. On the Diffusion of Acetonitrile in Nanoscale Amorphous Silica Pores. Understanding Anisotropy and the Effects of Hydrogen Bonding. *J. Phys. Chem. C* **117**, 19107-19114 (2013).

79. Borchardt L., Leistenschneider D., Haase J., Dvoyashkin M. Revising the Concept of Pore Hierarchy for Ionic Transport in Carbon Materials for Supercapacitors. *Adv. Energy Mater.* **8**, 1800892 (2018).

80. Koone N., Shao Y., Zerda T. W. Diffusion of Simple Liquids in Porous Sol-Gel Glass. *J. Phys. Chem.* **99**, 16976-16981 (2002).

81. Kittaka S. et al. Low Temperature Properties of Acetonitrile Confined in Mcm-41. *J. Phys. Chem. B* **109**, 23162-23169 (2005).

82. Nivarthi S. S., McCormick A. V., Davis H. T. Diffusion Anisotropy in Molecular Sieves. *Chem. Phys. Lett.* **229**, 297-301 (1994).

83. Natraj A. et al. Single-Crystalline Imine-Linked Two-Dimensional Covalent Organic Frameworks Separate Benzene and Cyclohexane Efficiently. *J. Am. Chem. Soc.* **144**, 19813-19824 (2022).